Author/s:
Zhong, Q;Li, S;Chen, J;Xie, K;Pan, S;Richardson, JJ;Caruso, F

Title:
Oxidation‐Mediated Kinetic Strategies for Engineering Metal–Phenolic Networks

Date:
2019-09-02

Citation:
Zhong, Q., Li, S., Chen, J., Xie, K., Pan, S., Richardson, J. J. & Caruso, F. (2019). Oxidation‐Mediated Kinetic Strategies for Engineering Metal–Phenolic Networks. Angewandte Chemie, 131 (36), pp.12693-12698. https://doi.org/10.1002/ange.201907666.

Persistent Link:
https://hdl.handle.net/11343/286187

Title: Oxidation-Mediated Kinetic Strategies for Engineering Metal–Phenolic Networks

Authors: Qi-Zhi Zhong; Shiyao Li; Jingqu Chen; Ke Xie; Shuaijun Pan; Joseph J. Richardson; Frank Caruso, Prof.

To be cited as: 10.1002/ange.201907666

Link to VoR: https://doi.org/10.1002/ange.201907666

Oxidation-Mediated Kinetic Strategies for Engineering Metal–Phenolic Networks

Qi-Zhi Zhong,[a] Shiyao Li,[a] Jingqu Chen,[a] Ke Xie,[b] Shuaijun Pan,[a] Joseph J. Richardson,[a] and Frank Caruso*[a]

Abstract: The tunable growth of metal–organic materials has implications for engineering particles and surfaces for diverse applications. Specifically, controlling the self-assembly of metal–phenolic networks (MPNs), an emerging class of metal–organic materials, is challenging, as previous studies suggest that growth often terminates through kinetic trapping. Herein, kinetic strategies are used to temporally and spatially control MPN growth by promoting self-correction of the coordinating building blocks through oxidation-mediated MPN assembly. The formation and growth mechanisms are investigated and used to engineer films with microporous structures and continuous gradients. Moreover, reactive oxygen species generated using ultrasonication expedite oxidation and result in faster (by ~30 times) film growth than that achieved by other MPN assembly methods. This study expands our understanding of metal–phenolic chemistry en route to engineering metal–phenolic materials for various applications.

Supramolecular metal–organic thin films have attracted interest owing to their diverse library of building blocks, hybrid physicochemical properties, and tunable responsiveness.[1] Additionally, a detailed understanding of the self-assembly process can allow for control over the resultant film structures and properties.[2] Recently, kinetic factors have been found to be important for synthesizing and controlling coordination-driven structures and functions. For example, the assembly kinetics can strongly influence the mode of molecular packing, where different synthesis pathways can often lead to distinct self-assembled structures with unique morphologies and functions.[3]

Metal–phenolic networks (MPNs) are an emerging class of functional coordination materials with a rich choice of metal ions and phenolic ligands.[4] Because of their strong adhesion to different substrates, diverse applicable building blocks, and tunable degradability, MPNs have recently garnered considerable attention.[5] Through either thermodynamic control at high temperature or kinetic assembly at low temperature, metals and phenols can self-assemble into crystalline or amorphous materials, respectively.[4d,6] For example, we reported a versatile method for conformally coating various surfaces with amorphous MPNs at room temperature.[6] Using the conventional MPN film preparation methodology (discrete adsorption from solution, i.e., discrete assembly),[6] film growth is rapid (<1 min), resulting in films with a thickness of ~10 nm and large pores (>6 nm), irrespective of the ligand, metal, or assembly conditions used.[7] However, this rapid, seemingly uncontrolled film growth creates challenges to engineer films with specific properties for various applications, including separations, drug delivery, sensing, and catalysis.

The discrete film growth[6] of MPNs is believed to occur due to a combination of factors, including kinetic trapping and symmetry breaking at the interface (i.e., low reversibility and low level of self-correction). These processes lead to the inclusion of defects and voids in the growing material and subsequent termination of the film growth when the defects arise on the surface.[8] Reversibility and self-correction are important for the continuous growth of large crystalline materials (e.g., metal–organic frameworks and covalent organic frameworks (COFs)) with specific size and morphology, as defects can lead to the termination of crystal growth.[9] For example, Ma et al. have reported that the slow imine-exchange strategy can increase the reversibility and self-correction of imine-based COFs and thus facilitates the formation of large single crystals.[10]

Herein, we investigate the use of kinetic strategies to engineer and expedite the controlled growth of amorphous MPN films. As a proof of concept, the oxidation-mediated coordination (OMC) assembly was examined as a strategy because it affords slow, yet continuous film growth.[11] Different from the discrete assembly process in which Fe^{III} metal salts, for instance, are used for formation, OMC assembly involves the use of Fe^{II} precursors, where the latter functions as a modulator that oxidizes to Fe^{III} during the growth process to stabilize the films (Scheme 1). Firstly, Fe^{II} is less reactive and less stable (stability constant, log $K_1 \approx 8$) than Fe^{III} (log $K_1 \approx 20$) toward coordination with catecholate complexes.[12] This lower reactivity and lower stability thus inhibit instantaneous coordination of Fe^{II} to the polyphenol (e.g., tannic acid (TA)) and potentially enhances the reversibility of the coordination linkages of TA and Fe^{II} owing to the dynamic nature of the coordination bonds. Secondly, the gradual conversion of TA–Fe^{II} to TA–Fe^{III} and low concentration of free TA–Fe^{III} complexes could provide additional opportunities for conformation adjustment and self-correction. Thirdly, owing to the higher solubility of Fe^{II} when compared with that of Fe^{III} (Fe^{III} tends to form μ-oxo-bridged species in aqueous media, see Figure S1), Fe^{II} is more accessible to the phenolic ligands, resulting in a higher degree of cross-linking in the networks.[7a,11b,13] Overall, both the coordination process and subsequent oxidation of TA–Fe^{II} to TA–Fe^{III} are dependent on time and concentration (i.e., kinetically controlled), ultimately affording temporal and spatial control over the thickness and microstructure of the MPN films.

Specifically, we demonstrate that by regulating the oxidation rate of TA–Fe^{II} to TA–Fe^{III} via the generation of reactive oxygen

[a] Q.-Z. Zhong, S. Li, J. Chen, Dr. S. Pan, Dr. J. J. Richardson, Prof. F. Caruso
Centre of Excellence in Convergent Bio-Nano Science and Technology, and the Department of Chemical Engineering, The University of Melbourne
Parkville, Victoria 3010 (Australia)
E-mail: fcaruso@unimelb.edu.au
[b] Dr. K. Xie
Department of Chemical Engineering
The University of Melbourne
Parkville, Victoria 3010 (Australia)

Supporting information for this article is given via a link at the end of the document.

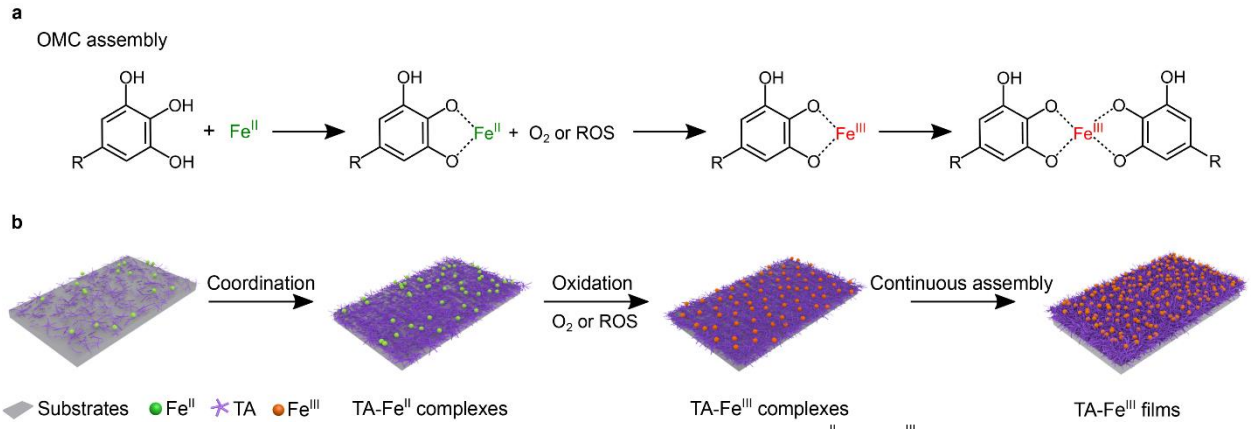

Scheme 1. OMC assembly for the continuous growth of MPNs. (a) Possible reactions of TA with Fe^{II} and Fe^{III}. (b) Schematic illustration of the continuous assembly of MPNs on planar substrates. ROS, reactive oxygen species.

species (ROS), the formation rate of the MPN films increased significantly, resulting in a growth rate of ~30 times faster than that achieved by other substrate-independent methods. Additionally, using the phenomena of the dissolved oxygen distribution in solution, the concentration of TA–Fe^{III} oxidized by molecular oxygen is distributed on a gradient from the oxygen source, and therefore MPN films with a gradient in thickness and transparency can be prepared. Notably, the films formed are microporous with a pore size of <1.7 nm as opposed to films obtained by the discrete assembly method (pore size > 6 nm). The kinetic and spatial control over the thickness and microstructure afforded by the method reported herein forms the basis for MPNs to be further engineered for specific applications.

We first investigated the fundamental differences between discrete assembly and OMC assembly in the process of film formation. Figure 1a shows that the color of the solution turned black instantly (~10 s) upon mixing the TA and $FeCl_3$ solutions (discrete assembly). The characteristic ligand-to-metal charge transfer (LMCT) band of TA/Fe^{III} at 565 nm rapidly plateaued (Figure 1a), suggesting that no new coordination was occurring in solution or on the film.[14] Numerous flocs appeared in solution (Figure S2), yet those flocs did not adhere to the substrate or form films.[11b] Even after 24 h, the MPN films prepared by discrete assembly were only ~10 nm in thickness with a root-mean-square (rms) roughness of ~2.8 nm (Figure 1c). In contrast, via the OMC assembly, the color of the mixed solution (TA and $FeCl_2$) gradually became blue–black, and the intensity of the LMCT band increased with time. This indicated continuous formation of TA–Fe^{III} complexes in solution. After 24 h, the thickness of the MPN films prepared via OMC assembly was ~120 nm, which is similar to the thickness achieved in a previous study using TA and $FeCl_2$ to form films at the air–water interface and stamping it onto a substrate.[11b] Energy-dispersive X-ray spectroscopy (EDS) results (Figure S3) confirmed the homogenous presence of Fe^{III} in the films, while X-ray photoelectron spectroscopy (XPS) (Figure S4) and UV–vis spectroscopy (Figure S5) confirmed the presence of TA–Fe^{III} complexes owing to the presence of the Fe 2p XPS peaks observed at binding energies of ~726 and 712 eV, which suggest Fe^{III} species, and the presence of the LMCT band of TA/Fe^{III} at 565 nm. Fourier transform infrared spectroscopy measurements (Figure S6) suggested the formation of coordination bonds between Fe^{III} and the phenolic hydroxyl groups in the films owing to the red shift of the C–O peaks from 1310 to 1330 cm^{-1}. Additionally, we noted that instead of the non-adhesive flocs formed by discrete assembly, OMC assembly produced globular aggregates (Figure S7) in solution. Atomic force microscopy (AFM) measurements (Figure 1d) confirmed the existence of nanoscale globular structures with a diameter of ~200 nm on the films, with an rms roughness of ~28 nm. This morphology was quite different from that of discrete MPN films. On the basis of these observations, we hypothesized that OMC assembly allows for the formation of metal–phenolic nanoparticles in solution. Such nanoparticles are adhesive and can then deposit on substrates to gradually grow into thick MPN films.

To confirm this hypothesis, the growth process of the MPN films and complexes in solution as a function of deposition time on polycarbonate (PC) membranes, as substrates, were monitored by scanning electron microscopy (SEM) and AFM. Before coating, the PC membranes featured ~0.1 μm pores on the surface (Figure 1f). After deposition of MPNs for 2 h, the pores of the PC membranes were partially covered by a thin layer (Figure 1g). Longer deposition times led to rougher MPN films with globular (50−100 nm in diameter) structures (Figure 1h). At 12 h, the globular structures in the films grew to 200−300 nm in diameter. This growth process was further confirmed by AFM measurements (Figure S8), which showed increasingly larger and higher globular structures on the surface over time. Furthermore, during the film growth process, the particles in solution and the globular structures in the films appeared to be similar in size (Figure S9).

The above observations provide valuable insights into the mechanism of MPN formation by the OMC assembly method. Firstly, the molecular TA–Fe^{III} complexes adsorb on the surface owing to the adhesion property provided by TA,[15] followed by the formation of a thin MPN layer on the substrate as shown in Figure 1e. Simultaneously, the precursors form metal–phenolic nuclei in solution. Owing to the slower assembly kinetics of this method, the self-correction of the dynamic coordination bonds potentially increases and subsequent premature termination decreases, which leads to the formation of nuclei complexes that

can continuously grow into particles in solution. The particles and

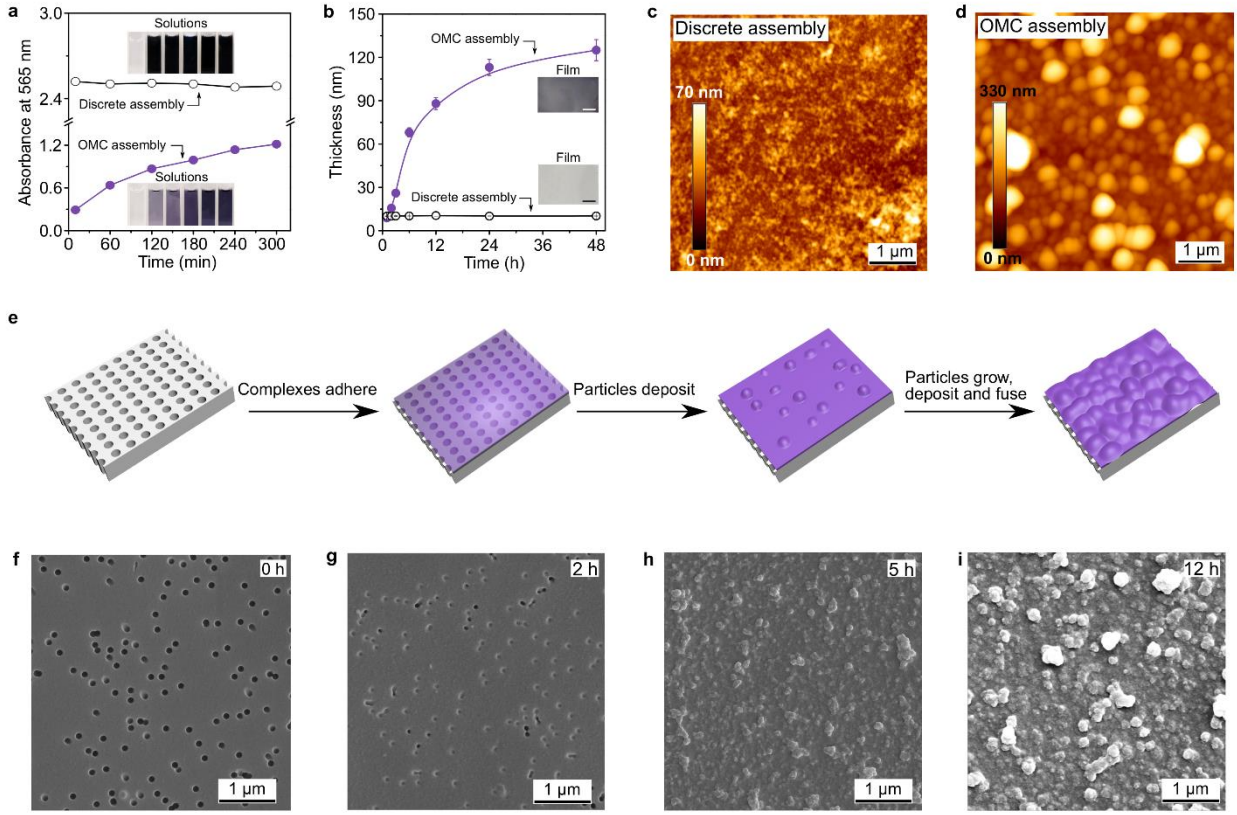

Figure 1. Formation of MPN films by the OMC assembly method on planar substrates. Comparison of (a) complex formation in solution, (b) growth of film thickness, and (c,d) morphology of MPN films prepared by the discrete[6] and OMC assembly methods. The insets in (a) show the change in color of the MPN solutions as the reaction proceeds. The insets in (b) show the MPN films formed on glass slides. Scale bars are 0.5 cm. (e) Schematic of MPN film formation process by the OMC assembly method. (f–i) SEM images of MPN films prepared by the OMC assembly method at different deposition times.

complexes then deposit, fuse, and grow into thick films driven by coordination, π–π stacking, and other noncovalent interactions.[15b] It is worth mentioning that though the discrete assembly method also produces nuclei in solution (Figure S10), the rapid kinetics can trap complexes in inefficient and defect-filled states, thus restricting self-correction. Moreover, the low solubility of Fe^{III} species in the process possibly inhibit further growth and rapidly cause the termination of the coordination reactions (Figure S11). Notably, the films in the form of capsules (Figure 2a) prepared via OMC assembly are significantly less permeable than MPN films prepared with discrete assembly,[6] and are impermeable even down to 5 kDa dextran (Figure 2b). This suggests that the films prepared by OMC assembly are capable of self-healing, as seen for other MPNs assembled with the help of oxidation,[11b] as the polymers (polystyrene templates) with a molecular weight of ~70 kDa need to pass through the MPN films during template removal.[6] The capsules are permeable to ethanol, indicating that the pore size of the film structure is between 0.44 to 1.66 nm.[16] This pore size range is significantly smaller than that of films prepared by discrete assembly (pore size > 6 nm). The microporous structure was further confirmed by the gas separation studies using hydrogen (H_2), nitrogen (N_2), and carbon dioxide (CO_2), wherein the H_2/CO_2 and H_2/N_2 selectivity values of the MPN films were 8.8 and 5.3, respectively (Figure 2c). The selectivity results obtained herein are well above the corresponding theoretical values for Knudsen diffusion (i.e., 4.7 for H_2/CO_2 and 3.7 for H_2/N_2), indicating a molecular sieving effect and the integration of the film.[17] Therefore, the kinetic assembly process occurring in the OMC assembly increases the integrity and connections of the coordination networks, leading to thicker, denser, and microporous MPN films.

With this understanding of the film growth process, we next attempted to control the thickness and microstructure of the MPN films, both of which are known to influence the performance of MPN-coated materials. To date, several methods have been reported for the continuous growth of MPN films including rust-mediated assembly, oxygen oxidation assembly, diffusion-driven assembly, and electro-triggered assembly.[7,11,18] These methods involve time-consuming steps or require specific substrates (e.g., conductive) to obtain thick (>30 nm) MPN films; however there is still a need to speed up the growth rate for thick MPN films. Herein, we demonstrate that the formation rate of MPN films can be accelerated in the presence of ROS generated by ultrasonication (Figure 3a). This method is independent of substrate properties yet allows for the generation of thick MPN films. The ROS are more active than molecular oxygen and can accelerate the oxidation rate of TA–Fe^{II} to TA–Fe^{III}.[19] Figure 3c shows that the thickness of the MPN films increased linearly with sonication time, reaching ~45

nm after only 15 min (Figure 3b, c and Figure S12). In contrast, using molecular oxygen as the oxidant, the films were only ~3 nm thick after 15 min (Figure 3c). Compared with other substrate-independent methods for preparing continuously grown

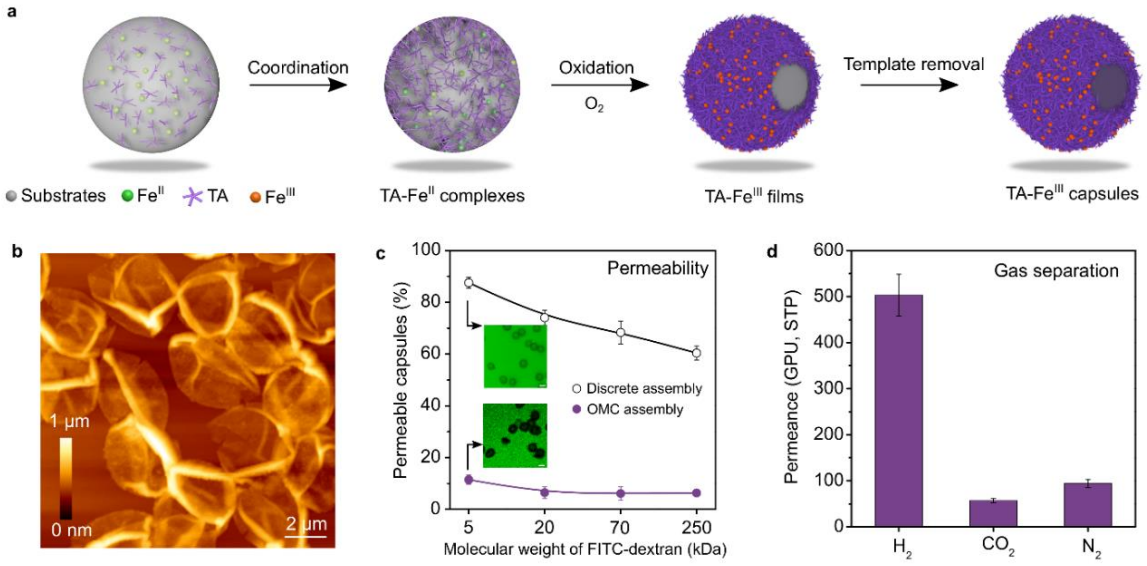

Figure 2. Microporous MPN films and capsules, and their application for gas separation. (a) Capsules prepared by the OMC assembly method. (b) Comparison of MPN permeability for capsules prepared by the discrete[6] and OMC assembly methods. The insets in (b) show confocal laser scanning microscopy images of the MPN capsules in fluorescein isothiocyanate (FITC)-dextran solution. Scale bars are 3 μm. (c) Gas permeance of H_2, N_2, and CO_2 through the microporous MPN films.

MPN films, the ROS oxidation method achieved the fastest deposition rate to date, i.e., ~180 nm h^{-1}, which is as high as 30 times that of other methods (Figure 3d).[7a,11b,18]

Not only can the film thickness be controlled by time, it can also be controlled spatially via the OMC assembly method. Because a concentration gradient spontaneously forms owing to the molecular diffusion of oxygen in aqueous solution under air,[20] we hypothesized that this oxygen distribution phenomena could be used to engineer MPN gradients on surfaces. To investigate this, substrates (e.g., silicon wafers) were immersed in a TA–$FeCl_2$ solution at 65°, as shown in Figure 3e. The oxygen concentration gradient influenced the oxidation of TA–Fe^{II} and subsequent nanoparticle formation. As a result, an MPN film with gradient thickness (5–13 nm, Figure 3g) and light absorbance (Figure 3h) was obtained. As opposed to other methods employed for preparing MPN gradients that are non-continuous,[21] our strategy can generate MPN films with continuous thickness gradients. The present strategy has potential for engineering

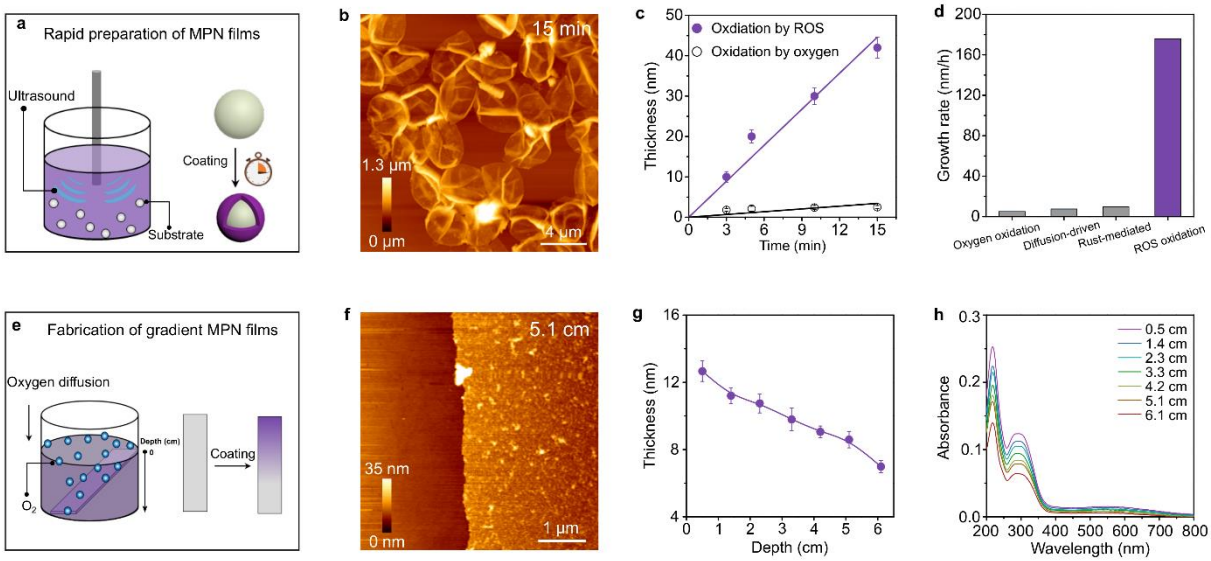

Figure 3. Temporal and spatial control of the thickness of MPN films prepared via the ROS oxidation method. (a) Schematic illustration of the rapid formation of MPN films in the presence of ROS generated from ultrasonication. (b) AFM image of MPN capsules prepared by ROS oxidation method after sonication for 15 min. (c) Time-dependence of MPN film thickness achieved in the presence of ROS and molecular oxygen. (d) Comparison of the formation rate of MPN films achieved by various substrate-independent growth methods. (e) Schematic of preparation of gradient MPN films in the presence of dissolved oxygen. (f) AFM image of MPN film at depth of 5.1 cm. (g) Depth-dependence of thickness of gradient MPN films and (h) corresponding absorbance profile.

biomimetic materials such as the jaw of polychaete worms which has exceptional mechanical properties owing to the presence of a continuous gradient of metal–organic networks.[22] Collectively, these results demonstrate that the OMC assembly method affords a strategy for kinetic control of MPN film thickness and microstructure in time and space.

The versatility of the present kinetic strategy in coating diverse substrates with different shapes included columnar substrates in addition to spherical and planar substrates (Figures 1–3, Figure S13). As shown in Figure S13, using oxygen as an oxidant, the color of the different substrate surfaces turned blue–black after 4 h. SEM, EDS, and AFM measurements confirmed the formation of conformal MPN coatings on these substrates, indicating that the unique universal adherence of MPNs is maintained using our strategy. Combined with the unique pH-tunable disassembly (Figure S14), our MPN capsules could be used in drug delivery, catalysis, and biosensing.[23] Moreover, the phenolic ligands and metal ions can be replaced with other phenols (e.g., gallic acid and pyrogallol, see Figure S15) and iron salts (e.g., $FeBr_2$ and $FeSO_4$, see Figure S16), respectively, for engineering MPN films, which further demonstrates the versatility and applicability of the OMC assembly strategy.

In conclusion, we demonstrated the use of kinetic strategies for engineering MPN films on various substrates. These kinetic strategies fundamentally influenced the formation process of MPN films, and as a result, the MPN growth process was controlled in time and space. We found that ROS, generated by ultrasonication, greatly sped up the growth process—a growth rate of ~30× faster than that achieved by other substrate-independent growth mechanisms. Moreover, we demonstrated the continuous growth of gradient films, which affords a unique means to fabricate asymmetric metal–organic films. Taken together, the kinetic strategies presented herein are facile and rapid toward the engineering of MPN films with desired thickness, microporous structures, and tunable disassembly on various surfaces. We expect that these developments will contribute toward a deeper understanding of MPN film growth, as well as broadening the application range of such materials.

Acknowledgements

This research was conducted and funded by the Australian Research Council Centre (ARC) of Excellence in Convergent Bio-Nano Science and Technology (project number CE140100036) and an ARC Discovery Project (DP170103331). F.C. acknowledges the award of a National Health and Medical Research Council Senior Principal Research Fellowship (GNT1135806).

Keywords: metal–organic films • polyphenols • reactive oxygen species • self-assembly • thin films

[1] a) N. Giuseppone, J. L. Schmitt, J. M. Lehn, *J. Am. Chem. Soc.* **2006**, *128*, 16748– 16763; b) D. Fujita, H. Yokoyama, Y. Ueda, S. Sato, M. Fujita, *Angew. Chem.* **2015**, *127*, 157–160; *Angew. Chem. Int. Ed.* **2015**, *54*, 155–158; c) C. Dietrich-Buchecker, B. Colasson, M. Fujita, A. Hori, N. Geum, S. Sakamoto, K. Yamaguchi, J. P. Sauvage, *J. Am. Chem. Soc.* **2003**, *125*, 5717–5725; d) T. R. Cook, P. J. Stang, *Chem. Rev.* **2015**, *115*, 7001–7045; e) R. Sakamoto, *Bull. Chem. Soc. Jpn.* **2017**, *90*, 272–278; f) M. Komiyama, K. Yoshimoto, M. Sisido, K. Ariga, *Bull. Chem. Soc. Jpn.* **2017**, *90*, 967–1004; g) V. Rubio-Giménez, M. Galbiati, J. Castells-Gil, N. Almora-Barrios, J. Navarro-Sánchez, G. Escorcia-Ariza, M. Mattera, T. Arnold, J. Rawle, S. Tatay, E. Coronado, C. Martí-Gastaldo, *Adv. Mater.* **2018**, *30*, 1704291; h) K. Ariga, D. T. Leong, T. Mori, *Adv. Funct. Mater.* **2018**, *28*, 1702905.

[2] Z. Y. Li, J. W. Dai, M. Damjanović, T. Shiga, J. H. Wang, J. Zhao, H. Oshio, M. Yamshita, X. H. Bu, *Angew. Chem.* **2019**, *131*, 4383–4388; *Angew. Chem. Int. Ed.* **2019**, *58*, 4339–4344.

[3] a) H. Kitagawa, H. Ohtsu, M. Kawano, *Angew. Chem.* **2013**, *125*, 12621–12625; *Angew. Chem. Int. Ed.* **2013**, *52*, 12395–12399; b) M. Kawano, T. Haneda, D. Hashizume, F. Izumi, M. Fujita, *Angew. Chem.* **2008**, *120*, 1289–1291; *Angew. Chem. Int. Ed.* **2008**, *47*, 1269–1271; c) Y. Yan, J. Huang, B. Z. Tang, *Chem. Commun.* **2016**, *52*, 11870–11884; d) A. K. Cheetham, G. Kieslich, H. H. Yeung, *Acc. Chem. Res.* **2018**, *51*, 659–667; e) M. Oh, C. A. Mirkin, *Nature* **2005**, *438*, 651–654.

[4] a) M. A. Rahim, S. L. Kristufek, S. Pan, J. J. Richardson, F. Caruso, *Angew. Chem.* **2019**, *131*, 1920–1945; *Angew. Chem. Int. Ed.* **2019**, *58*, 1904–1927; b) H. Ejima, J. J. Richardson, F. Caruso, *Nano Today* **2017**, *12*, 136–148; c) Q. Wei, R. Haag, *Mater. Horiz.* **2015**, *2*, 567–577; d) R. K. Feller, A. K. Cheetham, *Solid State Sci.*, **2006**, *8*, 1121–1125.

[5] a) M. A. Rahim, M. Björnmalm, T. Suma, M. Faria, Y. Ju, K. Kempe, M. Müllner, H. Ejima, A. D. Stickland, F. Caruso, *Angew. Chem.* **2016**, *128*, 14007–14011; *Angew. Chem. Int. Ed.* **2016**, *55*, 13803–13807; b) J. Guo, B. L. Tardy, A. J. Christofferson, Y. Dai, J. J. Richardson, W. Zhu, M. Hu, Y. Ju, J. Cui, R. R. Dagastine, I. Yarovsky, F. Caruso, *Nat. Nanotechnol.* **2016**, *11*, 1105–1111; c) Y. Shi, Y. Yu, Y. Liang, Y. Du, B. Zhang, *Angew. Chem.* **2019**, *131*, 3809–3813; *Angew. Chem. Int. Ed.* **2019**, *58*, 3769–3773; d) J. Wei, Y. Liang, Y. Hu, B. Kong, J. Zhang, Q. Gu, Y. Tong, X. Wang, S. P. Jiang, H. Wang, *Angew. Chem.* **2016**, *128*, 12658−12662; *Angew. Chem. Int. Ed.* **2016**, *55*, 12470–12474.

[6] H. Ejima, J. J. Richardson, K. Liang, J. P. Best, M. P. van Koeverden, G. K. Such, J. Cui, F. Caruso, *Science* **2013**, *341*, 154–156.

[7] a) M. A. Rahim, M. Björnmalm, N. Bertleff-Zieschang, Q. Besford, S. Mettu, T. Suma, M. Faria, F. Caruso, *Adv. Mater.* **2017**, *29*, 1606717; b) J. Kang, G. Bai, S. Ma, X. Liu, Z. Ma, X. Guo, X. Wang, B. Dai, F. Zhou, X. Jia, *Adv. Mater. Interfaces* **2019**, *6*, 1801789.

[8] a) M. A. Rahim, K. Kempe, M. Müllner, H. Ejima, Y. Ju, M. P. van Koeverden, T. Suma, J. A. Braunger, M. G. Leeming, B. F. Abrahams, F. Caruso, *Chem. Mater.* **2015**, *27*, 5825–5832; b) C. E. Lin, M. Y. Zhou, W. S. Hung, B. K. Zhu, K. E. Lee, L. P. Zhu, L. F. Fang, *Sep. Purif. Technol.* **2018**, *207*, 435–442.

[9] a) S. Dissegna, K. Epp, W. R. Heinz, G. Kieslich, R. A. Fischer, *Adv. Mater.* **2018**, *30*, 170450; b) N. Stock, S. Biswas, *Chem. Rev.* **2012**, *112*, 933–969; c) M. E. Belowich, J. F. Stoddart, *Chem. Soc. Rev.* **2012**, *41*, 2003–2024; d) E. Vitaku, W. R. Dichtel, *J. Am. Chem. Soc.* **2017**,

139, 12911–12914; e) S. Jiang, J. T. A. Jones, T. Hasell, C. E. Blythe, D. J. Adams, A. Trewin, A. I. Cooper, *Nat. Commun.* **2011**, *2*, 207.

[10] T. Q. Ma, E. A. Kapustin, S. X. Yin, L. Liang, Z. Y. Zhou, J. Niu, L. H. Li, Y. Y. Wang, J. Su, J. Li, X. G. Wang, W. D. Wang, W. Wang, J. L. Sun, O. M. Yaghi, *Science* **2018**, *361*, 48–52.

[11] a) C. Maerten, L. Lopez, P. Lupattelli, G. Rydzek, S. Pronkin, P. Schaaf, L. Jierry, F. Boulmedais, *Chem. Mater.* **2017**, *29*, 9668–9679; b) H. Lee, W. I. Kim, W. Youn, T. Park, S. Lee, T. S. Kim, J. F. Mano, I. S. Choi, *Adv. Mater.* **2018**, *30*, 1805091; c) B. J. Kim, J. K. Lee, I. S. Choi, *Chem. Commun.* **2019**, *55*, 2142–2145.

[12] N. R. Perron, H. C. Wang, S. N. DeGuire, M. Jenkins, M. Lawson, J. L. Brumaghim, *Dalton Trans.* **2010**, *39*, 9982–9987.

[13] a) J. Korać, D. M. Stanković, M. Stanić, D. Bajuk-Bogdanović, M. Žižić, J. B. Pristov, S. Grgurić−Šipka, A. Popović−Bijelić, I. Spasojević, *Sci. Rep.* **2018**, *8*, 3530; b) E. Nkhili, M. Loonis, S. Mihai, H. E. Hajji, O. Dangles, *Food Funct.* **2014**, *5*, 1186–1202.

[14] J. Guo, Y. Ping, H. Ejima, K. Alt, M. Meissner, J. J. Richardson, Y. Yan, K. Peter, D. von Elverfeldt, C. E. Hagemeyer, F. Caruso, *Angew. Chem.* **2014**, *126*, 5652–5627; *Angew. Chem. Int. Ed.* **2014**, *53*, 5546–5551.

[15] a) H. Lee, S. M. Dellatore, W. M. Miller, P. B. Messersmith, *Science* **2007**, *318*, 426–430; b) H. A. Lee, Y. Ma, F. Zhou, S. Hong, H. Lee, *Acc. Chem. Res.* **2019**, *52*, 704–713.

[16] P. Aimar, M. Meireles, V. Sanchez, *J. Membr. Sci.* **1990**, *54*, 321–338.

[17] a) F. Zhang, X. Zou, X. Gao, S. Fan, F. Sun, H. Ren, G. Zhu, *Adv. Funct. Mater.* **2012**, *22*, 3583–3590; b) Y. Hu, J. Wei, Y. Liang, H. Zhang, X. Zhang, W. Shen, H. Wang, *Angew. Chem.* **2016**, *128*, 2088–2092; *Angew. Chem. Int. Ed.* **2016**, *55*, 2048–2052; c) H. Bux, F. Liang, Y. Li, J. Cravillon, M. Wiebcke, J. Caro, *J. Am. Chem. Soc.* **2009**, *131*, 16000–16001.

[18] G. Yun, Q. A. Besford, S. T. Johnston, J. J. Richardson, S. Pan, M. Biviano, F. Caruso, *Chem. Mater.* **2018**, *30*, 5750–5758.

[19] a) X. Du, L. Li, J. Li, C. Yang, N. Frenkel, A. Welle, S. Heissler, A. Nefedov, M. Grunze, P. A. Levkin, *Adv. Mater.* **2014**, *26*, 8029–8033; b) C. Zhang, Y. Ou, W. X. Lei, L. S. Wan, J. Ji, Z. K. Xu, *Angew. Chem.* **2016**, *128*, 3106–3109; *Angew. Chem. Int. Ed.* **2016**, *55*, 3054–3057; c) F. Cavalieri, E. Colombo, E. Nicolai, N. Rosato, M. Ashokkumar, *Mater. Horiz.,* **2016**, *3*, 563–567.

[20] H. C. Yang, Q. Y. Wu, L. S. Wan, Z. K. Xu, *Chem. Commun.* **2013**, *49*, 10522–10524.

[21] Q. Z. Zhong, S. Pan, M. A. Rahim, G. Yun, J. Li, Y. Ju, Z. Lin, Y. Han, Y. Ma, J. J. Richardson, F. Caruso, *ACS Appl. Mater. Interfaces* **2018**, *10*, 33721–33729.

[22] a) J. A. Neal, N. J. Oldenhuis, A. L. Novitsky, E. M. Samson, W. J. Thrift, R. Ragan, Z. Guan, *Angew. Chem.* **2017**, *129*, 15781–15785; *Angew. Chem. Int. Ed.* **2017**, *56*, 15575–15579; b) H. C. Lichtenegger, T. Schoberl, M. H. Bartl, H. Waite, G. D. Stucky, *Science* **2002**, *298*, 389–392; c) J. D. Fox, J. R. Capadona, P. D. Marasco, S. J. Rowan, *J. Am. Chem. Soc.* **2013**, *135*, 5167–5174.

[23] a) W. Tong, X. Song, C. Gao, *Chem. Soc. Rev.* **2012**, *41*, 6103–6124; b) C. Yang, H. Wu, X. Yang, J. Shi, X. Wang, S. Zhang, Z. Jiang, *ACS Appl. Mater. Interfaces* **2015**, *7*, 9178–9184; c) L. Li, C. Yuan, D. Zhou, A. E. Ribbe, K. R. Kittilstved, S. Thayumanavan, *Angew. Chem. Int. Ed.* **2015**, *54*, 12991–12995; *Angew. Chem.* **2015**, *127*, 13183–13187.

COMMUNICATION

Kinetic assembly is an efficient strategy for rapidly and continuously growing metal-phenolic network materials. Using reactive oxygen species, films are grown ~30-fold faster than rates achieved using existing technologies. Furthermore, the films display unique microstructures and continuous film gradients, which are desirable properties for application in drug delivery and separations.

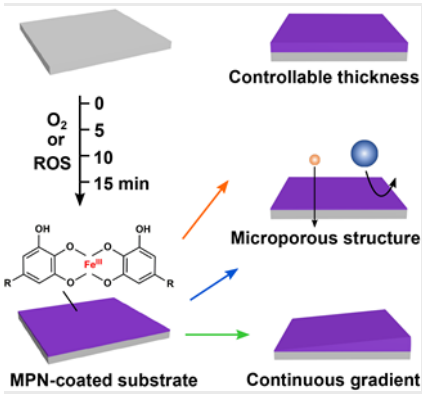

*Qi-Zhi Zhong, Shiyao Li, Jingqu Chen, Ke Xie, Shuaijun Pan, Joseph J. Richardson, Frank Caruso **

Page No. – Page No.

Oxidation-Mediated Kinetic Strategies for Engineering Metal–Phenolic Networks